# Secondary structure confirmation and localization of $Mg^{2+}$ ions in the mammalian CPEB3 ribozyme

MIRIAM SKILANDAT,[1] MAGDALENA ROWINSKA-ZYREK,[1,2] and ROLAND K.O. SIGEL
Department of Chemistry, University of Zurich, CH-8057 Zurich, Switzerland

## ABSTRACT

**Most of today's knowledge of the CPEB3 ribozyme, one of the few small self-cleaving ribozymes known to occur in humans, is based on comparative studies with the hepatitis delta virus (HDV) ribozyme, which is highly similar in cleavage mechanism and probably also in structure. Here we present detailed NMR studies of the CPEB3 ribozyme in order to verify the formation of the predicted nested double pseudoknot in solution. In particular, the influence of $Mg^{2+}$, the ribozyme's crucial cofactor, on the CPEB3 structure is investigated. NMR titrations, $Tb^{3+}$-induced cleavage, as well as stoichiometry determination by hydroxyquinoline sulfonic acid fluorescence and equilibrium dialysis, are used to evaluate the number, location, and binding mode of $Mg^{2+}$ ions. Up to eight $Mg^{2+}$ ions interact site-specifically with the ribozyme, four of which are bound with high affinity. The global fold of the CPEB3 ribozyme, encompassing 80%–90% of the predicted base pairs, is formed in the presence of monovalent ions alone. Low millimolar concentrations of $Mg^{2+}$ promote a more compact fold and lead to the formation of additional structures in the core of the ribozyme, which contains the inner small pseudoknot and the active site. Several $Mg^{2+}$ binding sites, which are important for the functional fold, appear to be located in corresponding locations in the HDV and CPEB3 ribozyme, demonstrating the particular relevance of $Mg^{2+}$ for the nested double pseudoknot structure.**

**Keywords: CPEB3; ribozyme; pseudoknot; $Mg^{2+}$; metal ion; NMR**

## INTRODUCTION

The discovery of small self-cleaving ribozymes in mammalian genomes is rather recent. Only in the last decade, a discontinuous hammerhead ribozyme in the 3′-UTR of C-type lectin type 2 genes (Martick et al. 2008), a hammerhead ribozyme in an intron of a tumor suppressor gene (de la Pena and Garcia-Robles 2010), the CoTC motif in the 3′-untranslated region of the β-globin gene (Teixeira et al. 2004) (although in a later work [Dye et al. 2006], autocatalytic RNA cleavage of the CoTC element in the context of intron 2 could not be confirmed), and the CPEB3 ribozyme in the second intron of the *cpeb3* gene (which encodes a cytoplasmic polyadenylation element binding protein) (Richter 2007) were described. In this study, we focus on the CPEB3 ribozyme, which was discovered via an in vitro selection approach, starting from a human genomic library (Salehi-Ashtiani et al. 2006).

The function of the CPEB3 ribozyme in the cell is yet unknown but it is likely to regulate the levels of the CPEB3 protein in the cell by its self-cleavage. The CPEB family of proteins is involved in diverse processes such as germ cell development and synaptic plasticity (Christerson and McKearin 1994; Lantz et al. 1994; Luitjens et al. 2000; Darnell and Richter 2012). A single nucleotide polymorphism (SNP) in the human CPEB3 ribozyme has been shown to alter the rate of self-cleavage and to influence episodic memory (Vogler et al. 2009). This supports the suggested correlation between ribozyme activity, CPEB3 protein concentration and learning and memory.

When the CPEB3 ribozyme's cleavage reaction was initially characterized, it became clear that its catalytic mechanism was very similar to that of the HDV ribozyme. The HDV ribozyme is involved in the separation of genome copies of the HDV satellite generated during rolling-circle replication (Macnaughton et al. 1993; Jeng et al. 1996). Both ribozymes cleave upstream of their first nucleotide, have nearly constant activity over a pH range of ~6 to 8.5, show a solvent kinetic isotope effect, require $Mg^{2+}$ for catalysis and are inhibited by hexamminecobalt(III) (Nakano et al. 2001; Salehi-Ashtiani et al. 2006). This strongly suggests that both ribozymes use a very similar combination of acid–base catalysis mediated

[1]**These authors contributed equally to this work.**
[2]**Present address: Faculty of Chemistry, University of Wrocław, 50-383 Wrocław, Poland**
**Corresponding author: roland.sigel@chem.uzh.ch**
Article published online ahead of print. Article and publication date are at http://www.rnajournal.org/cgi/doi/10.1261/rna.053843.115.

by their nucleobases and $Mg^{2+}$-assisted catalysis. Support for the mechanistic resemblance of both ribozymes comes from the fact that all CPEB3 ribozyme sequences can be folded (in silico) into the nested double pseudoknot structure, which is known to occur only in the HDV ribozyme (Fig. 1A). Moreover, the mutation of nucleotides in positions corresponding to catalytically relevant nucleotides of the HDV ribozyme, interferes with CPEB3 self-cleavage (Salehi-Ashtiani et al. 2006).

The nested double pseudoknot structure of the HDV ribozyme comprises two helices (P1 and P2), two hairpin structures (the internal P3 and the P4 hairpin) and two single-stranded linker regions J1/2 and J4/2 (Fig. 1A,B; Perrotta and Been 1991; Ferre-D'Amare et al. 1998) and is required for self-cleavage activity of both the genomic and antigenomic forms (Wadkins et al. 1999). A small pseudoknot consisting of P3 and P1.1 is embedded in a larger one consisting of P1 and P2. Based on the most recent crystal structure and molecular dynamics studies of the HDV ribozyme, a reverse G·U wobble base pair has been suggested to be formed at the base of P3 (G25·U20 wobble, circled residues on Fig. 1; Krasovska et al. 2006; Chen et al. 2010; Veeraraghavan et al. 2011; Kapral et al. 2014), which was not observed in the first two crystal structures (Ferre-D'Amare et al. 1998; Ke et al. 2004). This G25·U20 wobble is assumed to position the catalytic $Mg^{2+}$ ion in the active site, which comprises also C75, the catalytic cytosine (C57 in the CPEB3 ribozyme) (Chen et al. 2013). N3-protonated C75 has been proposed to act as the general acid in the cleavage mechanism that protonates the 5′-O leaving group with an estimated p$K_a$ of 6.4 (Gong et al. 2007). The catalytic $Mg^{2+}$ ion has recently been proposed to serve as Lewis acid, Brønsted base, or both to activate the 2′-OH nucleophile, as well as to coordinate to the pro-$R_P$ oxygen of the scissile phosphodiester (Chen et al. 2013; Thaplyal et al. 2013).

The strong resemblance of the CPEB3 and HDV ribozymes with regard to their catalytic reactions and (suggested) secondary structures has inspired the idea that the ribozymes are evolutionarily related, despite their dissimilar sequences. Given that the CPEB3 sequence is conserved in mammals, and that HDV is infecting humans, it seems most probable that the CPEB3 ribozyme is evolutionarily young and has been passed from human to HDV (Webb et al. 2009; Webb and Luptak 2011).

Although the complicated nested double pseudoknot motif is unlikely to have arisen independently several times (Nix et al. 1999; Nehdi and Perreault 2006), extensive bioinformatic searches have discovered the motif in the genomes of many organisms such as insects, nematodes, an insect virus, and bacteria. These HDV-like ribozymes are not conserved in their sequences and vary greatly in the length and structure of L1/2 and P4 (Webb et al. 2009; Webb and Luptak 2011; Riccitelli et al. 2014). This argues for the nested double pseudoknot motif being frequently used in self-cleaving sequences.

The HDV and CPEB3 ribozymes are different from all other small ribozymes in their obligatory requirement for divalent metal ions in their catalytic mechanism (Murray et al. 1998). This study, which is one of two NMR studies of such a full-length nested double pseudoknot construct (Tanaka et al. 2002), validates the proposed structure of the CPEB3 ribozyme in solution and elucidates the role of $Mg^{2+}$ for structure formation. The constructs used were the human and chimpanzee (Fig. 1B) sequence of the ribozyme, which differ in only one nucleotide in P1 (G30 → A). A partial assignment

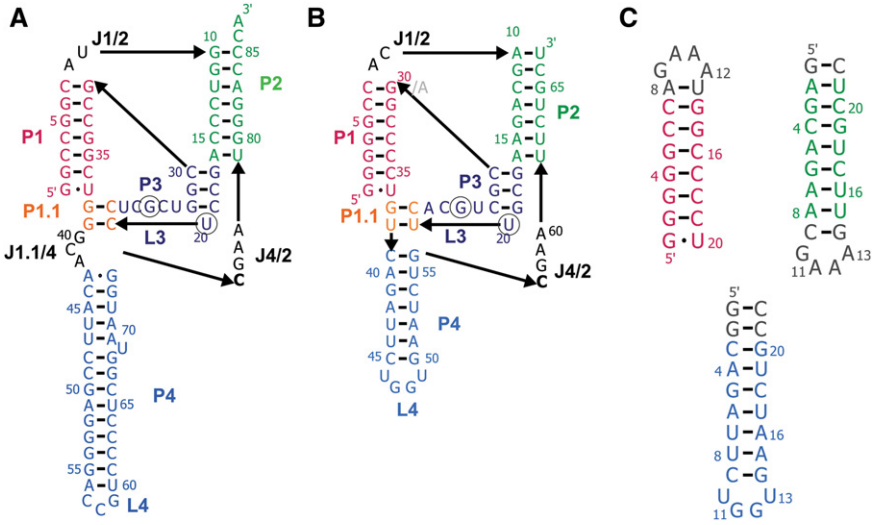


**FIGURE 1.** Secondary structures of the genomic HDV ribozyme (*A*), the chimpanzee CPEB3 ribozyme (*B*), and the small model constructs P1, P2, and P4 (*C*) used for resonance assignment. P1 is shown in red, P1.1 in orange, P2 in green, P3 and L3 in dark blue, and P4 in light blue; the J1/2 and J4/2 linkers are shown in black, the catalytic cytosine is in boldface; the two nucleotides G25·U20 that form a wobble pair only in the presence of $Mg^{2+}$ (for the CPEB3 ribozyme, see far infra) are circled in *A* and *B*; in *B*, the difference between the chimpanzee and human sequence is shown in gray (G30A substitution); (*C*) the nucleotides added to the natural sequences of P1, P2, and P4 are shown in gray.

of the CPEB3 proton and nitrogen resonances was obtained using three model hairpin constructs for P1, P2, and P4 (Fig. 1C). We have used NMR, $Tb^{3+}$-induced cleavage and ion counting techniques for a detailed investigation of $Mg^{2+}$ binding to the CPEB3 ribozyme. Our results are compared to the crystal structures of the HDV ribozyme, confirming strong structural parallels of both ribozymes and shedding light on the critical role of site-specific $Mg^{2+}$ binding for the native fold.

## RESULTS

### The wild-type human and chimpanzee CPEB3 ribozyme constructs are catalytically active

To confirm that the ribozyme constructs were self-cleaving, we performed cotranscriptional cleavage studies of the human and the chimpanzee sequences, which were elongated by 18 nt of the native genomic sequence on the 5′-end. In vitro transcription reactions were stopped after different time intervals and the cleavage products were separated and analyzed on denaturing PAGE gels (Fig. 2). Both constructs self-cleave, as evidenced by the band of the post-cleavage ribozyme control (67mer) and a band corresponding to the cleaved 18mer that intensifies with time. Also, the two DNA template strands, the 24mer (TS) and the 107mer (OT) are visible. The band of the uncleaved 85mer ribozyme is also detected but it is much less intense than the post-cleavage ribozyme, which indicates that the majority of molecules are active. Consequently, the 67mer constructs used in the structural and metal ion binding studies can indeed be derived from ribozyme self-cleavage and therefore are likely to represent the native fold of the post-cleavage ribozyme.

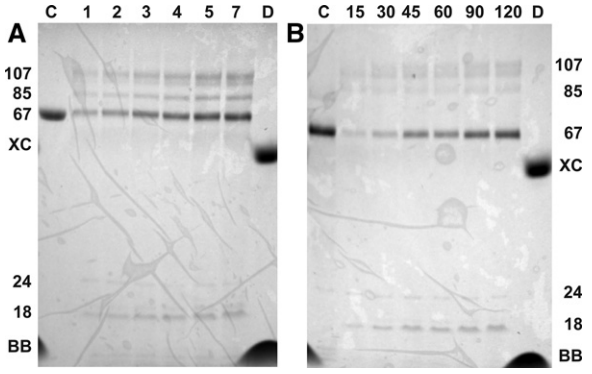


**FIGURE 2.** Cotranscriptional self-cleavage assay of a 5′-elongated human (*A*) and chimpanzee (*B*) CPEB3 ribozyme sequence. In vitro transcription/cleavage reactions were left to proceed for 1–7 h or 15–120 min for the human and chimpanzee sequence, respectively. The incubation time (*A* in hours, *B* in minutes) is specified on *top* of the lanes. Lane *C* contains the control sequence as in Figure 1B, transcribed from a non-elongated template. Lane *D* contains the two dyes bromophenol blue (BB) and xylene cyanol (XC). In addition, major bands in the transcription lanes are labeled with the putative lengths of constructs, i.e., uncleaved ribozyme (85mer), post-cleavage ribozyme (67mer), and the cleaved 18mer. Two further bands in the transcription lanes correspond to the double-stranded DNA template, the *top* strand TS (24mer) and the template strand OT (107mer).

The self-cleavage rates of the human (Fig. 2A) and chimpanzee (Fig. 2B) sequences are distinctly different, although their sequences differ only in nucleotide 30, which is a G in the chimpanzee and an A in the human sequence, the chimpanzee one seems to cleave at least four times faster. This is in agreement with previous studies, which explain the lower cleavage rate of the human sequence by a higher propensity of mispairing between P1/P1.1 and the upstream sequence (Chadalavada et al. 2010).

### NMR confirms the HDV-like secondary structure

NMR proton resonance assignment of the CPEB3 ribozyme proved to be challenging because of the severe spectral overlap in the [$^1$H,$^1$H]-NOESY spectra, which is mainly due to the large size of the ribozyme. The chimpanzee construct was chosen for NMR studies, as its spectra looked slightly better resolved compared to the human one (probably due to the canonical base-pairing which additionally stabilizes the P1 helix in the chimpanzee construct [C7–G30, see Fig. 1]). All other experiments ($Tb^{3+}$-induced cleavage, DOSY NMR and ion-counting techniques) were performed on the human CPEB3 ribozyme.

Assignments were made on partially deuterated CPEB3 RNA in the absence of $Mg^{2+}$, in which the signal overlap is drastically alleviated. The assignment was supported by the following strategies: (i) G,C, or A,U-$^{13}$C, $^{15}$N-labeled RNA or uniformly $^{15}$N-labeled RNA helped to identify [$^1$H,$^1$H]-NOESY or [$^1$H,$^{15}$N]-HSQC correlations belonging to certain nucleotides; (ii) four samples containing only one natural abundance nucleotide (with the remaining three being fully deuterated); and (iii) three small model constructs for the P1 and P2 helices and for the P4 hairpin (Fig. 1C) were produced and analyzed to confirm the assignment of the CPEB3 ribozyme spectra. Combining these data, the majority of the nonexchangeable H1′, H2′, H6/8, H2 proton resonances, encompassing the 5′ strand of P1, P2, P3, P4, and the J4/2 linker, were assigned (Supplemental Table S1). Assignments for J1/2, L3 and P1.1, regions from the center of the ribozyme, could not be obtained. Comparison of the proton chemical shifts of the three model constructs and the full-length CPEB3 ribozyme reveal that P4 chemical shifts are in excellent agreement (Skilandat et al. 2014). The chemical shift values of the P1 and P2 model constructs only approximate those of P1 and P2 within the ribozyme, however, the relative arrangement of chemical shifts within the sequences is the same (Supplemental Figs. S1, S2; Supplemental Tables S2, S3).

For the three long helical domains, P1, P2, and P4, imino protons and nitrogens were fully assigned (Figs. 3, 4; Supplemental Table S1) and all [$^1$H,$^1$H]-NOE cross peaks, which are expected from the model constructs could be attributed in the CPEB3 ribozyme (Fig. 3). Please note that in the

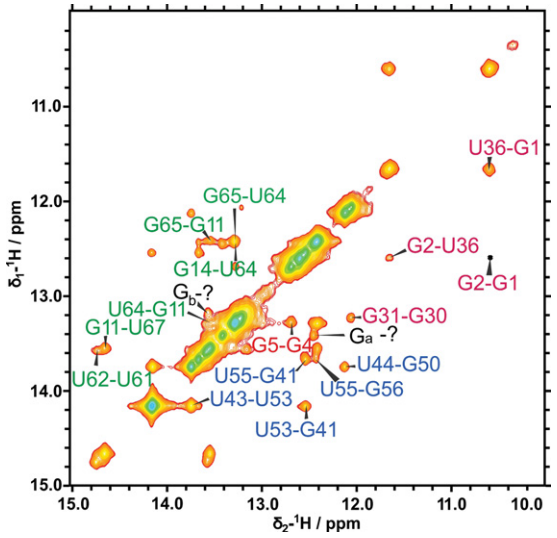


**FIGURE 3.** Imino proton region of the [$^1$H,$^1$H]-NOESY of the exchangeable protons of the chimpanzee CPEB3 ribozyme. The cross peaks are labeled in the color corresponding to the ribozyme domain. The spectrum was recorded at 278 K in $H_2O$ (100 mM KCl, 10 µM EDTA, pH 6.8). Note that there is no indication for the G20·U25 wobble pair in the absence of $Mg^{2+}$.

discussion below, the nucleotide numbering corresponds to the full-length construct (not to auxiliary helices). Typical NOEs for A-helical arrangements including also several stacking interactions were observed in the NOESY spectra of nonexchangeable protons of P1, P2, and P4 regions. Moreover, characteristic features such as the upfield shifted and very similar H8 chemical shift values of G2 to G5 and their similar and downfield shifted H1′ resonances as well as the far upfield shifted A13H2 and G14H8 are observed both within the CPEB3 ribozyme and in the P1 and P2 model constructs (Supplemental Figs. S1, S2; Supplemental Tables S1–S3). Such upfield shifts are indicative of stacking interactions between the nucleobases and are thus typically found in stable helices. Taken together, the data clearly demonstrate that the longer P1, P2, and P4 helices are formed and base paired according to the proposed secondary structure.

The formation of those helices is additionally confirmed by a $J_{NN}$ HNN-COSY experiment (Fig. 4), which makes use of the *N*,*N* coupling across the hydrogen bond as a direct reporter for base pair formation. Except for the signals belonging to G–C base pairs in P1, P2, and P4, three additional peaks that correspond to G–C base pairs are present ($G_a$, $G_b$, and $G_c$, Fig. 4; please note that exactly three G–C base pairs are expected in the small P3 helix). Two of the respective imino protons also show NOE cross peaks, which could, however, not be assigned to specific Gs or Cs, due to the lack of conclusive NOE cross peaks (Fig. 3). The presence of the additional imino signals, together with the high upfield shift of G17H8 and a G17H8–C18H6 cross peak, which suggest stacking interactions and the formation of a stable helix, are an indication that the P3 helix might be formed. Assuming that is the case, then the most likely reason for the lack of sequential NOEs is conformational dynamics in P3 and L3/P1.1, which would also explain why we could not assign any NOE correlations for L3 and P1.1. Given that L3 is mostly unpaired and P1.1 also contains one G–C and a less stable U–U base pair, a flexibility of this region is quite probable.

Internucleotide H2′(*n*)-H6/8(*n* + 1) and H1′(*n*)-H6/8 (*n* + 1) NOE cross peaks are observed throughout the 4-nt long J4/2 linker, which contains the active site cytosine. While the lack of further NOEs prohibits a more detailed view on the structure of this linker, the presence of these sequential-walk resonances suggests a rather stable assembly of the J4/2 linker nucleotides stacked on top of each other.

## $Mg^{2+}$ is required for a compact fold of the CPEB3 ribozyme

As $Mg^{2+}$ is known to be required by many RNAs to adopt their native structure, and is obligatory for CPEB3 activity, we first assessed the influence of $Mg^{2+}$ on the global structure of the CPEB3 ribozyme. Using Diffusion Ordered SpectroscopY (DOSY) NMR experiments, $K^+$ and $Mg^{2+}$ titrations of the ribozyme were performed to determine changes in the hydrodynamic radius ($r_H$) upon addition of different amounts of metal ions (Table 1). The theoretical $r_H$ of the CPEB3 ribozyme can only be estimated based on the related HDV ribozyme architecture: We assume that the folded ribozyme has a length *a*, which corresponds to 19 base pairs, i.e., the sum of base pairs in P2, P3, P4, and P1.1, and a width *b* of about twice the diameter of an A-form helix. With 0.26 nm and 2.4 nm being the distance between two base pairs and the diameter of a standard A-form RNA, respectively,

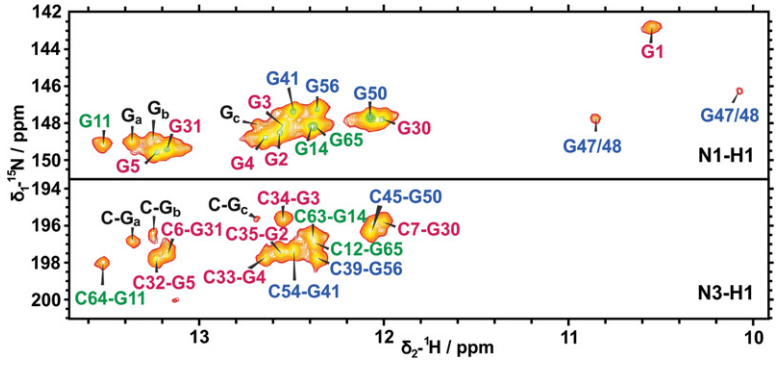


**FIGURE 4.** $J_{NN}$ HNN-COSY of the chimpanzee CPEB3 ribozyme imino groups. The peaks are labeled in the color corresponding to the ribozyme domain. The spectrum was recorded at 278 K in $H_2O$ (100 mM KCl, 10 µM EDTA, pH 6.8).

**TABLE 1.** Hydrodynamic radii ($r_H$) of the human CPEB3 ribozyme in different concentrations of $K^+$ and $Mg^{2+}$

| $[K^+]$/mM | $[Mg^{2+}]$/mM | $r_H \pm 1\ \sigma$/nm |
|---|---|---|
| 0 | 0 | 3.91 ± 0.03 |
| 10 | 0 | 3.38 ± 0.03 |
| 100 | 0 | 2.83 ± 0.01 |
| 100 | 2 | 2.56 ± 0.02 |
| 100 | 5 | 2.53 ± 0.02 |
| 100 | 10 | 2.45 ± 0.02 |
| 100 | 20 | 2.44 ± 0.02 |

All $r_H$ values are arithmetic means of three integrated regions with one standard deviation. DOSY spectra were acquired in $D_2O$, pD 6.8, 298 K.

$a = 18{\cdot}0.26$ nm = 4.68 nm, and $b = 2{\cdot}2.4$ nm = 4.8 nm. Because $b/a < 2$, a spherical model can be applied, in which $r_H$ is defined as half of the length (Eimer et al. 1990; Lapham et al. 1997). Consequently, $r_H$ should be between 2.34 nm and 2.4 nm as a first estimate.

CPEB3 does not achieve the native fold in the absence of significant amounts of counter ions (Table 1): The large hydrodynamic radius of 3.91 nm in the absence of salt is probably an averaged value of different extended states. Also, 10 mM $K^+$ are not sufficient for the ribozyme to obtain a compact fold, which is not surprising, considering the intricate pseudoknot topology of CPEB3. A significant compaction is only achieved in the presence of 100 mM $K^+$ (2.83 nm), but the addition of small concentrations of $Mg^{2+}$ further reduces the $r_H$ (2.56 nm in 2 mM $Mg^{2+}$). $[Mg^{2+}] > 2$ mM further decrease $r_H$ until above 10 mM $Mg^{2+}$ no significant change of the 2.45 nm hydrodynamic radius can be observed anymore. Reannealing of the ribozyme after the addition of $Mg^{2+}$ did not affect the measured $r_H$, indicating that the compact, $Mg^{2+}$-bound ribozyme structure is accessible without prior melting of base pairs.

The hydrodynamic radii determined in the presence of 100 mM $K^+$ and 10–20 mM $Mg^{2+}$ (2.44–2.45 nm) are very close to the above estimated value (2.4 nm, based on a similar core architecture as the HDV ribozyme). Based on the significant decrease in $r_H$ upon addition of $Mg^{2+}$, we conclude that $Mg^{2+}$ is necessary for the ribozyme to reach its native fold. A recent study, which used cleavage studies and SAXS to test the impact of molecular crowding agents on the size and activity of the human CPEB3, showed that the dimension of the ribozyme in 10 mM $Mg^{2+}$ is the same as the one measured in the presence of 0.5 mM $Mg^{2+}$ and molecular crowding agents (Strulson et al. 2013). This finding suggests that the size of the CPEB3 ribozyme in 10 mM $Mg^{2+}$ corresponds to the one under physiological conditions.

## Locating $Mg^{2+}$ binding sites by NMR spectroscopy

Having established that $Mg^{2+}$ ions are necessary to reach the native fold of the ribozyme, we located the binding sites of this metal ion and assessed, whether inner- or outer-sphere binding occurs at each site. The term "inner-sphere" describes a direct coordination of $Mg^{2+}$ to the RNA, e.g., to N7 of guanine or to the nonbridging phosphate oxygens (Freisinger and Sigel 2007; Sigel and Pyle 2007). Outer-sphere coordination, in contrast, is mediated by water ligands in the first coordination shell of the $Mg^{2+}$ ion. The latter can be probed using hexamminecobalt(III), $[Co(NH_3)_6]^{3+}$, as an exchange-inert substitute of hexaaquamagnesium(II) (Rowinska-Zyrek et al. 2013).

$Mg^{2+}$ binding is detected through chemical shift changes and by line broadening of the proton resonances in $[^1H,^1H]$-NOESY spectra. In the case of $[Co(NH_3)_6]^{3+}$, NOE cross peaks between the protons of the amine ligands and the coordinating nucleotide can be observed (Robinson and Wang 1996; Rowinska-Zyrek et al. 2013). $Mg^{2+}$ titrations were performed with the partially deuterated CPEB3 RNA (Fig. 5; Supplemental Fig. S3; Supplemental Table S1), as well as with the four samples containing one natural abundance and three fully deuterated nucleotides, and with the P1, P2, and P4 constructs (data not shown). All titrations showed consistent results. Nonexchangeable $[^1H,^1H]$-NOESY spectra show that six regions are strongly affected by the addition of $Mg^{2+}$: (i) the central part of the P2 helix (G11–C12 and A13H2 broaden to baseline, A13–G14 H8 and H1′ and G65–C66 H1′ and H2′ [from the opposite side of the strand] broaden and shift, Fig. 5A; Supplemental Table S1); the (ii) J4/2 linker with the catalytic C57, of which the respective cross peaks (C57-A59) are broadened to baseline at 5 mM $Mg^{2+}$, indicating a strong interaction (Fig. 5A); (iii) A60H8 in the upper part of the J4/2 linker is not broadened, but strongly shifted (0.273 ppm, Fig. 5A; Supplemental Table S1). Proton resonances of (iv) the base pairs adjacent to the P4 tetraloop (G50, A51), (v) in the P4 stem (A40, G41) and (vi) in the P1 stem (G3–G5) also display pronounced chemical shift changes (Fig. 5A; Supplemental Table S1).

To probe the above described $Mg^{2+}$ binding sites for possible outer-sphere coordination, $[^1H,^1H]$-NOESY spectra of the nonexchangeable (data not shown) and exchangeable protons were recorded in the presence of 1.5 mM $[Co(NH_3)_6]^{3+}$ (Fig. 5B, purple spectrum). The $[Co(NH_3)_6]^{3+}$ protons show cross peaks to G2H1, G4H1, G5H1 (Fig. 5B), and G5H8 (data not shown) of P1, suggesting that the P1 stem prefers outer-sphere binding. More NOE cross peaks are observed between the protons of $[Co(NH_3)_6]^{3+}$ and G41H8, C54H6, and U55H3 in P4, demonstrating outer-sphere coordination to the P4 stem. $[Co(NH_3)_6]^{3+}$ does not show cross peaks to the $Mg^{2+}$ binding sites in P2 and in the L4 tetraloop. Consequently, $Mg^{2+}$ binding to these sites requires a partial dehydration of the $Mg^{2+}$ ion. The position and coordination preference of both binding sites in the P4 domain are in line with what has been observed in the P4 model construct (Skilandat et al. 2014). In the J4/2 linker, cross peaks to the $[Co(NH_3)_6]^{3+}$ protons are only observed for A60H1′ and A60H8, suggesting

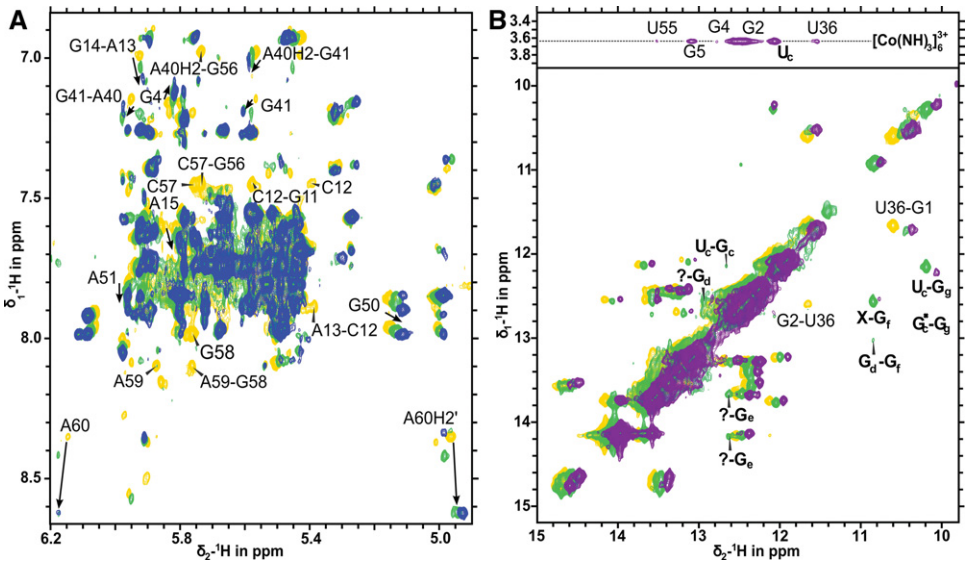


**FIGURE 5.** Metal ion-induced changes in the [$^1$H,$^1$H]-NOESY correlations of the chimpanzee CPEB3 ribozyme. (*A*) Superposition of the [$^1$H,$^1$H]-NOESY spectrum of nonchangeable protons in the absence of $Mg^{2+}$ (yellow), in the presence of 5 mM $Mg^{2+}$ (green), and 9 mM $Mg^{2+}$ (blue). Cross peaks with highly pronounced shifts and cross peaks broadened below the detection limit are labeled. Resonances in F2 belong to H1′ and resonances in F1 belong to H6/8 unless otherwise indicated. The spectra were recorded at 298 K in $D_2O$ (100 mM KCl, 10 µM EDTA, pD 6.8). (*B*) $Mg^{2+}$ and $[Co(NH_3)_6]^{3+}$ binding to the imino protons. Superposition of [$^1$H,$^1$H]-NOESY spectra recorded in the absence of metal ions (yellow), in the presence of 5 mM $Mg^{2+}$ (green, shifted by –0.08 ppm in F2), and in the presence of 1.5 mM $[Co(NH_3)_6]^{3+}$ (purple, shifted by –0.16 ppm in F2). Upon addition of $Mg^{2+}$, new cross peaks appear (labeled in boldface). The *upper* part contains the spectral region, in which cross peaks between $[Co(NH_3)_6]^{3+}$ and RNA protons are located. The spectra were recorded at 278 K in $H_2O$ (100 mM KCl, 10 µM EDTA, pH 6.8).

that the 3′ part of the linker is involved in an outer-sphere binding site, whereas the 5′ part preferentially binds $Mg^{2+}$ in an inner-sphere manner, which is expected for the active site cytosine (Nakano et al. 2001; Gong et al. 2007, 2009). The [$^1$H,$^1$H]-NOESY spectra of the exchangeable protons in the presence of $Mg^{2+}$ or $[Co(NH_3)_6]^{3+}$ reveal another binding site at the G1·U36 wobble base pair. This site is identified by broadening of the cross peaks involving U36H3 and G1H1 and G2H1 and by an NOE between U36H3 and the protons of $[Co(NH_3)_6]^{3+}$ (Fig. 5B).

In total, up to eight sites in the CPEB3 ribozyme are affected by $Mg^{2+}$: (i) the tetraloop of P4, (ii) the upper half of the P2 helix, and (iii) the nucleotides surrounding C57 prefer inner-sphere coordination of $Mg^{2+}$. The (iv) G1·U36 wobble, (v) the upper part of the P4 helix, and (vi) A60 located in the upper part of the J4/2 linker can also accommodate outer-sphere coordinated $Mg^{2+}$, whereas (vii) the middle part of the P1 stem seems to be the only site that prefers $[Co(NH_3)_6]^{3+}$ over $Mg^{2+}$. The eighth and probably one of the most important $Mg^{2+}$ binding sites, the G25·U20 wobble, is discussed in the paragraph below.

## $Mg^{2+}$-induced structural changes

In the [$^1$H,$^1$H]-NOESY spectrum in 90% $H_2O$ as well as in the [$^1$H-$^{15}$N]-TROSY spectrum, new peaks appear upon addition of $Mg^{2+}$ (bold labels in Figs. 5B, 6A). Judging by their $^{15}$N chemical shifts, these new peaks correspond to four guanines ($G_d$, $G_e$, $G_f$, $G_g$) and five uracils ($U_a$, $U_b$, $U_c$, $U_d$, $U_e$). There are six guanines (G17, G19, G25, G28, G37, and G58), and four uracils (U20, U21, U26, U38) in the sequence, whose imino protons and nitrogens were not yet conclusively assigned. Given that another three guanine resonances, $G_a$, $G_b$, and $G_c$ (suggested to be the three Gs from the P3 helix), were already observed in the absence of $Mg^{2+}$ in the $J_{NN}$ HNN-COSY (Fig. 4) or NOESY (Fig. 3), there is at least one surplus correlation of both a uracil and a guanine, possibly as a result of conformational exchange. Four of the six unassigned guanine H1 are located in G–C base pairs ($G_a$, $G_b$, $G_c$, and $G_e$) (Fig. 6B). This is an important finding, given that exactly four G–C base pairs are expected to be formed for P3 and P1.1, according to the proposed secondary structure (Fig. 1B). We hence assigned the newly appearing guanines and uracils based on the [$^1$H,$^1$H]-NOESY correlations as far as possible.

The most intense cross peak that appears in the presence of $Mg^{2+}$ (and also in the presence of $[Co(NH_3)_6]^{3+}$) is the one between a GH1 and a UH3 ($U_c$–$G_g$ resonance, Fig. 5B). The $U_c$–$G_g$ NOE cross peak is in a position that is typical for a G·U wobble pair. As the formation of an extra G·U wobble at the base of the P3 helix has been suggested for the HDV ribozyme (Krasovska et al. 2006; Chen et al. 2010; Veeraraghavan et al. 2011; Kapral et al. 2014), we speculated that the corresponding G25·U20 wobble forms as well in the CPEB3 ribozyme upon addition of $Mg^{2+}$, giving rise to the observed NOE correlation. The hypothesis was both tempting and probable, however it longed for more substantial evidence, since theoretically, also other scenarios might

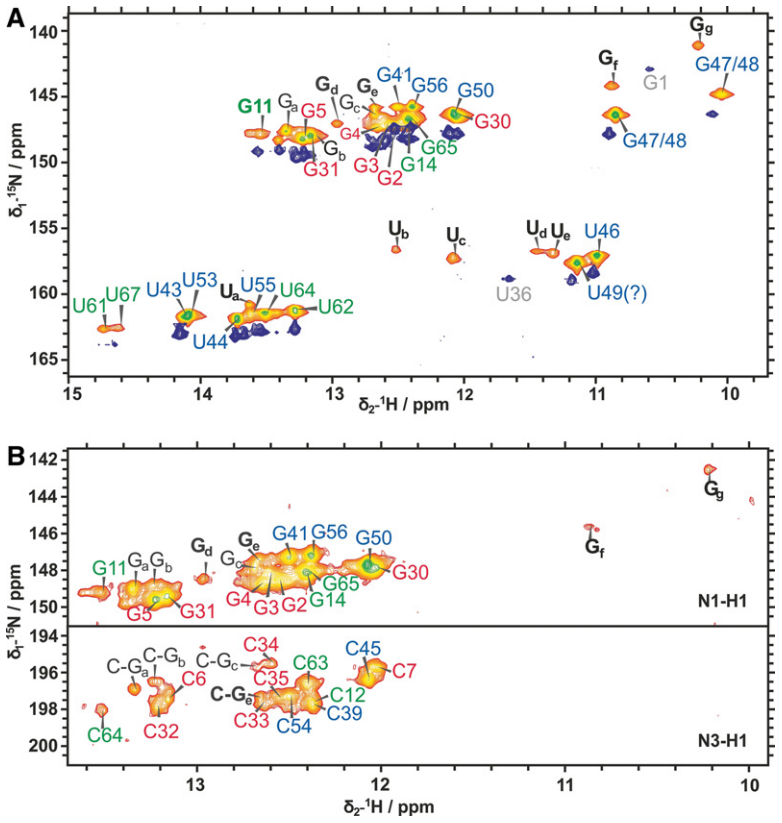


**FIGURE 6.** $Mg^{2+}$-induced changes in the [$^1$H,$^{15}$N]-TROSY (*A*) and the $J_{NN}$ HNN-COSY (*B*) of the imino groups of the chimpanzee CPEB3 ribozyme. (*A*) The spectrum in the presence of 5 mM $Mg^{2+}$ is shown in orange-green and is superimposed with the spectrum recorded in the absence of $Mg^{2+}$ (blue, shifted by 1.5 ppm in F1 for better comparison). In *A* and *B*, peaks that appear after the addition of 5 mM $Mg^{2+}$ are labeled in bold; resonances that disappear after the addition of $Mg^{2+}$ are labeled in gray. All spectra were recorded at 278 K in $H_2O$ (100 mM KCl, 10 µM EDTA, pH 6.8).

have been occurring, such as, e.g., the formation of a G19·U26 wobble. To test our theory, we studied the imino proton behavior of a U20C mutant, both in the presence and absence of $Mg^{2+}$ ions. In monovalent metal ions only, the mutant seems to form the same base-pairing interactions as the wild-type CPEB3 construct (also, no canonical C20–G25 base pair is formed, or the signal is overlapped with other cross peaks). In the presence of 5 mM $Mg^{2+}$, no additional peaks appear (Supplemental Fig. S4) and a further increase of $Mg^{2+}$ concentration does not cause any changes, apart from a general broadening of observed signals. This clearly confirms that in the case of the wild-type construct, the $U_c$·$G_g$ resonance which appears in the presence of magnesium(II) is indeed the U20·G25 wobble. This is an important finding which again shows a structural and functional similarity between the CPEB3 and HDV ribozymes—in the HDV ribozyme, this G·U wobble is thought to present the catalytically active $Mg^{2+}$ ion to the active site cytosine (Chen et al. 2010). This correlates well with our finding that this signal is only visible after the addition of $Mg^{2+}$. $U_c$H3, now assigned to U20H3, has a strong cross peak to the $[Co(NH_3)_6]^{3+}$ protons. Since the G·U wobble in the active site of the HDV ribozymes makes outer-sphere contacts to $Mg^{2+}$ with its minor groove, the observed cross peak is in agreement with our suggested assignment.

Although the presence of the $U_c$, $G_c$, $G_e$, $G_g$, and $U_a$ cross peaks suggests the formation of the small P3–P1.1 pseudoknot (according to the proposed secondary structure) and strong evidence suggests that $U_c$·$G_g$ is the substantial U20·G25 wobble (see above), there are too few cross peaks to relate the imino protons within P3 to other helices. We suspect that the combined effects of $Mg^{2+}$-induced line broadening and of flexibility in the P3–P1.1 pseudoknot cause the low intensity or lack of NOE correlations. One argument for the flexibility is the fact that at least two surplus NH correlations are observed in the [$^1$H,$^{15}$N]-TROSY spectrum (Fig. 6A). Another feature that might indicate conformational exchange is the prominent X–$G_f$ cross peak appearing upon $Mg^{2+}$ addition (Fig. 5B). X is either a uracil ($U_b$) or a guanine overlapped with G41, according to the TROSY correlations (Fig. 6A). Both X and $G_f$ are correlated to another unpaired guanine $G_d$. It is not clear which nucleotides could give rise to this cross peak, as the sequence does not contain unpaired guanines close to each other. It is thus possible that X–$G_f$ is not actually an NOE but an exchange cross peak between two different conformations of the same proton.

Beyond any doubt, $Mg^{2+}$, apart from binding to the previously described sites in P1, P2, and P4, has a very strong influence on the nucleotides in the remaining ribozyme domains, forming the inner pseudoknot and active site. $Mg^{2+}$ induces a gain of structure in this region by enabling additional internucleotide contacts or by stabilizing them. This is in perfect agreement with the overall compaction of the ribozyme, which was observed in the presence of $Mg^{2+}$ and it again underlines the importance of this metal ion for the structure and function of the CPEB3 ribozyme.

## $Tb^{3+}$-induced cleavage reveals metal ion binding in the P3–P1.1 pseudoknot

$Tb^{3+}$-induced RNA cleavage experiments were carried out in order to confirm the $Mg^{2+}$ binding sites determined from the NMR titration data and to obtain information on metal ion binding sites in the inner pseudoknot (P1.1, P3, L3) of the

CPEB3 ribozyme, where the lack of resonance assignment prevents an NMR study of the metal ion binding sites.

$Tb^{3+}$ can be used to map $Mg^{2+}$ binding sites in RNA through hydrolytic cleavage experiments (Ciesiolka et al. 1989; Sigel and Pyle 2003; Erat and Sigel 2011; Choudhary et al. 2014). Lanthanide ions are assumed to be good mimics of $Mg^{2+}$, since they occupy the same binding sites in RNA molecules, but bind with an at least three orders of magnitude higher affinity (Kayne and Cohn 1974; Sigel and Pyle 2003; Erat and Sigel 2011). In a $Tb^{3+}$-induced cleavage experiment, $Tb^{3+}$ is added to a folded ribozyme, where it binds to RNA, displacing the previously bound $Mg^{2+}$ ions. The partially deprotonated $Tb^{3+}$ aqua-complex deprotonates the 2′-OH of a close-by nucleotide, which enables a nucleophilic attack of the 2′-oxyanion on the adjacent phosphodiester bond. This triggers backbone scission and the resulting fragments can be separated by PAGE and visualized to identify the metal ion binding sites (Fig. 7; Choudhary et al. 2014).

$Tb^{3+}$-induced cleavage of the human CPEB3 ribozyme takes places in three main regions: the P2 helix (C12), the P4 tetraloop (G48), and several positions in the core of the ribozyme encompassing P1.1, P3, L3, J4/2, and the upper part of P4. The most intense cleavage bands correspond to those of the junction of P4 to J4/2 (G56, C57, G58) and to P1.1 (C22) and L3 (U20, A23). While the P2 stem and L4 clearly represent two distinct binding sites, the number of binding sites in the P1.1–P3 pseudoknot cannot be determined, as the distance and relative orientation of the affected nucleotides in the folded structure are not known (Fig. 7). However, judging by the number of affected nucleotides and the secondary structure, we estimate two to four ions to bind to the ribozyme core comprising the active site and the P1.1–P3 pseudoknot.

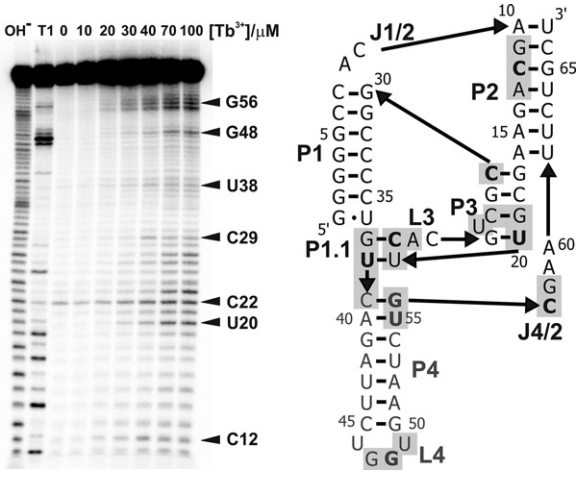


**FIGURE 7.** $Tb^{3+}$-induced hydrolytic cleavage sites in the human CPEB3 ribozyme indicate sites of $Mg^{2+}$ binding. The ribozyme was incubated with different concentrations of $TbCl_3$ (indicated on *top* of the gel) for 30 min at 298 K. The resulting ribozyme fragments were separated by PAGE. The positions that correspond to the observed cleavage sites were determined with the help of the $OH^-$ hydrolytic cleavage ladder (first lane) and the T1 enzymatic cleavage ladder (second lane). The nucleotides most strongly cleaved at 40 μM $Tb^{3+}$ are indicated in bold. Regions of additional nucleotides being cleavage at this concentration are marked with a gray background.

The binding sites obtained from $Tb^{3+}$-induced cleavage confirm $Mg^{2+}$ binding to L4, J4/2, and the P2 stem, which was detected by NMR spectroscopy. The binding sites of $[Co(NH_3)_6]^{3+}$ in the P4 and P1 stem are not occupied by $Tb^{3+}$. This is probably due to different local structures being required for $[Co(NH_3)_6]^{3+}$ binding and for permitting a $Tb^{3+}$-induced cleavage reaction (Soukup and Breaker 1999).

## Counting bound $Mg^{2+}$ ions

We used two different ion counting methods to independently estimate the number of $Mg^{2+}$ ions bound to the CPEB3 ribozyme. The first method uses the dye 8-hydroxyquinoline-5-sulfonic acid (HQS), whose 1:1 $Mg^{2+}$–HQS complex is fluorescent (Romer and Hach 1975; Grilley et al. 2009). In the second method, equilibrium dialysis of the RNA sample with a known concentration of free $Mg^{2+}$, followed by an atomic absorption spectroscopy (AAS) measurement of total $Mg^{2+}$ concentration of both solutions is used (Bina-Stein and Stein 1976; Das et al. 2005; Leipply et al. 2009).

For our measurements, both methods gave corresponding values within error limits, showing that the four $Mg^{2+}$ ions are associated with the CPEB3 ribozyme. This number seems to be independent of the concentration of monovalent ions in the buffer. At 100 mM KCl, fluorescence titrations yielded 4.13(±0.32) $Mg^{2+}$ ions bound to the ribozyme, while dialysis results suggested that 3.95(±0.25) $Mg^{2+}$ ions bound. At 50 mM KCl, 4.36(±0.24) and 4.41(±0.05) $Mg^{2+}$ ions were detected by the fluorescence and dialysis methods, respectively. A drastically increased concentration of monovalent ions did not significantly alter the result. At 2 M KCl the number of bound ions detected by fluorescence is 4.33 (±0.08), and 3.96 as determined by equilibrium dialysis and AAS (Table 2).

The fact that four bound $Mg^{2+}$ ions are counted in the presence of different concentrations of $K^+$ indicates that these four ions are site-bound with higher affinity and occupancy factors and less diffusion into the surrounding ion cloud (Das et al. 2005). Probably, they are bound to specific sites in noncanonical regions in the center of the ribozyme, which are at least partially protected from the bulk solvent, i.e., in the catalytic core of the enzyme (around C57) and the inner P1.1–P3 pseudoknot.

## DISCUSSION

In this study, we demonstrate that the post-cleavage CPEB3 ribozyme adopts its global fold in monovalent ions alone but that $Mg^{2+}$ binding to several sites is required to fully

**TABLE 2.** Number of $Mg^{2+}$ ions bound to CPEB3

| | $Mg^{2+}$:CPEB3 ratio | |
|---|---|---|
| $[K^+]$/mM | Equilibrium dialysis | HQS fluorescence |
| 50 | 4.41 ± 0.05 | 4.36 ± 0.24 |
| 100 | 3.95 ± 0.25 | 4.13 ± 0.32 |
| 2000 | 3.96[a] | 4.33 ± 0.08 |

Values represent arithmetic means and errors of a series of measurements from two individual experiments.
[a]Only one measurement was performed.

form the inner pseudoknot, active site, and the compact native structure. The P1–P2 pseudoknot and the P4 domain of the ribozyme are base paired according to the HDV-like secondary structure proposed earlier (Salehi-Ashtiani et al. 2006), independent of the presence of $Mg^{2+}$. These structures (P1, J1/2, P2, P4, and J4/2) account for the largest part of the ribozyme sequence (52 of 67 nt, 21 of 26 predicted base pairs) and are constrained in their orientation due to the short linkers in between the helices. Accordingly, the overall fold of the CPEB3 ribozyme is largely determined by base-pairing and thus corresponds to the one of the HDV ribozyme, which is subject to very similar structural constraints.

So far, the extent to which the inner pseudoknot is formed is not entirely clear. Judging by the number of G–C correlations in the $J_{NN}$ HNN-COSY, probably P3 is at least partially formed in the absence of $Mg^{2+}$. Nevertheless, the addition of $Mg^{2+}$ has a very pronounced effect on the CPEB3 structure and is known to be strictly required for catalysis (Salehi-Ashtiani et al. 2006). Unfortunately, the severe line broadening upon addition of $Mg^{2+}$ prevents a detailed pH titration study to investigate a possible shifted p$K_a$ for C57, as has been suggested for the HDV ribozyme (Gong et al. 2007). However, $Mg^{2+}$ significantly reduces the ribozyme's hydrodynamic radius at near-physiological concentrations and binds to several sites in the ribozyme, thereby promoting the formation of additional structure in the catalytic core. Our data provide strong evidence that the full predicted secondary structure (Salehi-Ashtiani et al. 2006) is formed only in the presence of $Mg^{2+}$. This includes the G25·U20 wobble at the base of P3 and the smaller P1.1–P3 pseudoknot, but that the latter retains some flexibility. This is in line with the data on the HDV ribozyme, whose L3 region has been shown to be mobile, a feature that is probably meaningful for self-cleavage activity (Krasovska et al. 2006). The outer-sphere coordination mode of $Mg^{2+}$ bound to the G25·U20 wobble is another common feature for the CPEB3 and HDV ribozymes (Nakano et al. 2001).

To clarify the structural role of $Mg^{2+}$ in the CPEB3 (and HDV) ribozyme, we now discuss the metal ion binding sites we have observed in more detail and compare them to those observed in the HDV ribozyme crystal structures (Fig. 8). Our NMR data show evidence for the formation of an outer-sphere $Mg^{2+}$ binding to the G·U wobble base pair (G25·U20). A corresponding $Mg^{2+}$ is supposed to take part in active site formation in the HDV ribozyme ($Mg^{2+}$ [1] in Fig. 8A,B, red nucleotides in Fig. 8C). As this site presumably presents the catalytic, outer-sphere bound $Mg^{2+}$ ion to the catalytic cytosine and the scissile bond between −1 nucleotide and G1, it is possible that the strong line broadening effect that we observe for C57 and G58 as well as the $Tb^{3+}$-induced cleavage band at C57 are due to the same metal ion. Also, the $Tb^{3+}$-induced cleavage bands at C22 and A23, which according to the HDV crystal structure are in direct vicinity (Fig. 8A), may result from $Tb^{3+}$ binding to the active site. This binding site illustrates very well the double role of $Mg^{2+}$ in structure and function for this ribozyme. Apart from its role in the catalytic mechanism, it also stabilizes the interaction of three different regions of the secondary structure being the J4/2 linker, the P1 terminus, and the base of the P3 helix.

The second $Mg^{2+}$ binding site of possible structural relevance for the CPEB3 and the HDV ribozymes lies between the sugar–phosphate backbones of the two adenines in J4/2

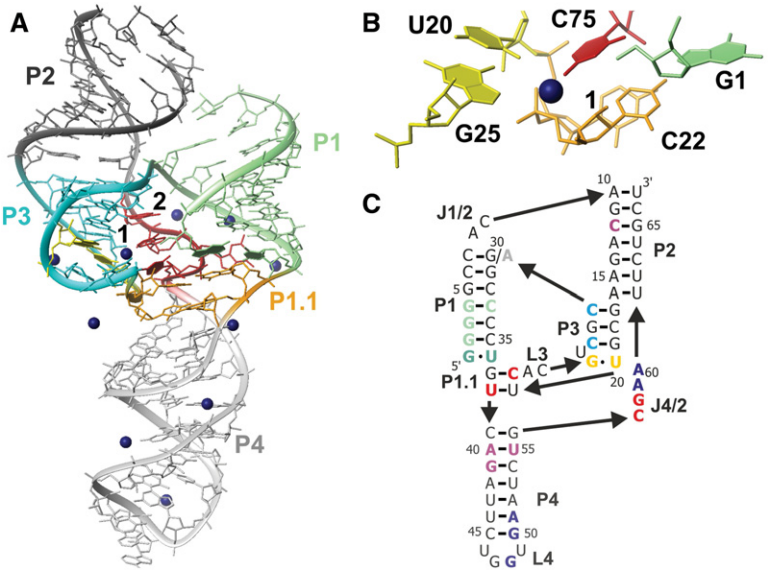


**FIGURE 8.** Location of metal ion binding sites in the HDV and human CPEB3 ribozymes. (*A*,*B*) Crystal structure of the inhibited HDV ribozyme, pdb entry 3NKB (Chen et al. 2010): Full structure (*A*) and a close up (*B*) of the active site. $Mg^{2+}$ ions are shown as dark blue spheres, J4/2 is shown in red, and the G25·U20 wobble formed only in the presence of $Mg^{2+}$ is shown in yellow. (*C*) $Mg^{2+}$ binding sites in the CPEB3 ribozyme. Each color represents a different binding site. The difference between the chimpanzee and human sequence (G30A substitution) is shown in gray.

and the P1 stem in the HDV crystal structure ($Mg^{2+}$ [2] in Fig. 8A, blue nucleotides in Fig. 8C). We have demonstrated $[Co(NH_3)_6]^{3+}$ (and to a lesser extent $Mg^{2+}$) binding to the corresponding sites of the CPEB3 ribozyme. $[Co(NH_3)_6]^{3+}$ inhibits ribozyme activity indicating that at least one partially dehydrated $Mg^{2+}$ is needed. The coordination of such a partially dehydrated $Mg^{2+}$ in this location might help to overcome backbone repulsion between J4/2 and P1, which is another aspect of how $Mg^{2+}$ can promote the formation of a compact native structure of both CPEB3 and HDV. Also, the outer-sphere binding site at the G1·U36 wobble (khaki nucleotides in Fig. 8C) (G1–U37 in HDV) occurs in both ribozymes and has been suggested to stabilize the P1.1 minihelix (Veeraraghavan et al. 2011), which maintains stacking interactions with P1. Probably, there are further binding sites for $Mg^{2+}$ in the core region of the CPEB3 ribozyme (orange and green-blue nucleotides in Fig. 8C), which requires stabilization due to the higher content of unpaired bases and the proximity of the different backbone segments. The binding sites in P2 and P4 (yellow, green, and violet nucleotides in Fig. 8C) are more likely to stabilize local structure such as the UGGU tetraloop (Skilandat et al. 2014) because these regions should not be in direct contact with other domains. In conclusion, a direct comparison of $Mg^{2+}$ binding sites in CPEB3 and HDV ribozymes is not as straightforward as it might seem because sites that stabilize the local structures of separate helices are not conserved, as are the sequences of those helices not conserved. On the contrary, sites that are involved in the stabilization of the pseudoknot or that are necessary for catalysis, bind $Mg^{2+}$ ions both in the case of the HDV and the CPEB3 ribozyme.

The question remains, which are the four binding sites that we counted in the CPEB3:$Mg^{2+}$ stoichiometry experiments? As these ions remain bound in up to 2 M KCl, they are tightly bound to sites, which are at least partly shielded from the solvent or offer a favorable geometry for inner-sphere contacts between the RNA and the $Mg^{2+}$ ion (Das et al. 2005). Accordingly, the three binding sites in the stem of P1, P4, and at the G1·U36 wobble (blue, green, and khaki nucleotides in Fig. 8C) are unlikely to be counted, because they can accommodate outer-sphere coordination and, judged by the HDV ribozyme crystal (Fig. 8) and the P4 NMR structure (Skilandat et al. 2014) are accessible for the solvent. It is not possible to univocally determine which metal ion binding sites are detected by the ion counting. Based on our combined data, we hypothesize that one of them is between the active site cytosine C57 and the G25·U20 wobble, and the second one is also in the core of the structure, possibly between the sugar–phosphate backbones of the two adenines in J4/2 and the P1 stem. The two remaining binding sites could be located in the P2 stem and P4 tetraloop (yellow and violet nucleotides in Fig. 8C). Both sites offer a suitable geometry for inner-sphere coordination of $Mg^{2+}$ and this type of binding could be thermodynamically and kinetically more stable. It is remarkable that a comparably small structure such as the CPEB3 RNA contains four such high-affinity sites, and underscores the extraordinary significance of $Mg^{2+}$ for the particular structure and mechanism of this ribozyme.

The CPEB3 and HDV ribozymes are different from all other small ribozymes investigated so far in that they crucially depend on the presence of divalent metal ions for catalysis, both in low and in high concentrations of monovalent ions. Also, their nested double pseudoknot fold is far more complicated than the secondary structures of the other small ribozymes. The data presented here (i) confirm that the CPEB3 ribozyme folds the same way as the related HDV and (ii) illustrate why the $Mg^{2+}$ dependence does not only stem from the catalytic mechanism but is inherent to the particular structure of the CPEB3 and HDV ribozymes, by completely structuring their inner catalytic core.

## MATERIALS AND METHODS

DNA oligonucleotide templates of the human and chimpanzee CPEB3 ribozymes and their corresponding elongated, precleavage constructs were purchased from Microsynth. Natural abundance, partially deuterated and fully deuterated nucleoside 5′-triphosphates were purchased from GE Healthcare and Cambridge Isotope Laboratories and uniformly $^{15}N$-labeled and $^{13}C$, $^{15}N$-labeled nucleotides from Silantes. The T7 RNA polymerase used for in vitro transcription was produced in house according to standard procedures (Gallo et al. 2005). $[Co(NH_3)_6]Cl_3$ and 8-hydroxyquinoline-5-sulfonic acid were purchased from Sigma Aldrich and 100% $D_2O$ was purchased from Armar Chemicals. The electroelution apparatus Elutrap was from Whatman. For desalting, Vivaspin Concentrators (5000 MWCO for the full-length constructs and 2000 MWCO for the auxiliary short ones) from Sartorius-Stedim biotech were used. Thermosensitive shrimp alkaline phosphatase and T4 polynucleotide kinase as well as the appropriate buffers were purchased from Promega.

### Cotranscriptional self-cleavage assays of CPEB3

In vitro transcription reactions with an elongated 107mer DNA template (designed to transcribe into the CPEB3 ribozyme with additional 18 nucleotides at the 5′ end) were performed in aliquots of 40 µL in the presence of 5 mM $Mg^{2+}$. For human and chimpanzee CPEB3, single aliquots were removed after 1, 2, 3, 4, 5, and 7 h or 15, 30, 45, 60, 90, and 120 min, respectively, and immediately frozen in liquid nitrogen to stop both transcription and cleavage. All samples were then centrifuged for 15 s and a mixture of 82% formamide and 10 mM EDTA was added to the supernatant (1:1). The transcription/cleavage products were subsequently separated by 12% denaturing PAGE.

### NMR sample preparation

All constructs were synthesized by in vitro transcription with T7 polymerase from a double-stranded DNA template (Gallo et al. 2005). Reaction mixtures typically contained 4.5–6 mM of each NTP, 0.9–1.2 µM of each strand of the synthetic, PAGE-purified, double-stranded DNA template, 30–50 mM $MgCl_2$, 40 mM Tris–HCl

(pH 7.5), 40 mM DTT, 2 mM spermidine, and 0.01% Triton X. The amount of T7 RNA polymerase was adapted according to activity of each enzyme batch. Transcription was allowed to proceed at 37°C for 6 h. The transcribed RNA was purified by denaturing 12% PAGE, UV-shadowed, excised from the gel, and recovered by electroelution. During ultrafiltration in Vivaspin devices, the RNA was washed repeatedly with 2 M KCl, pH 8 to remove Tris and afterward several times with water. After lyophilization, the sample was dissolved in 250 µL $D_2O$ or 90% $H_2O$, 10% $D_2O$ containing an appropriate amount of KCl (100 mM for CPEB3 and P1, 20–50 mM for P2 and P4) and 10 µM EDTA. The pH was adjusted to 6.8 in $H_2O$ or 6.4 in $D_2O$, corresponding to a pD of 6.8 (Glasoe and Long 1960). The RNA concentration of the samples varied between 0.4 and 0.9 mM and was determined on a Varian Cary 100 Scan UV-Vis spectrometer by using extinction coefficients of $\varepsilon_{260}$ of 203.4 $mM^{-1}$ $cm^{-1}$ (P1), 212 $mM^{-1}$ $cm^{-1}$ (P2), and 725 $mM^{-1}$ $cm^{-1}$ (CPEB3). Before acquisition of NMR data, all samples were annealed by 2-min incubation at 90°C, followed by rapid cooling in ice water.

## NMR spectroscopy

All spectra were recorded on a Bruker Avance 600 MHz spectrometer with a 5 mm CRYO TCI inverse triple-resonance probehead with *z*-gradient coil or on a Bruker Avance 700 MHz spectrometer with a 5-mm CRYO TXI inverse triple-resonance probehead with *z*-gradient coil. All samples contained 0.4–0.9 mM of sample being either natural abundance RNA, partially deuterated ([5, 3′, 4′, 5′, 5′′]-$^2$H) RNA, a combination of fully deuterated and wild-type RNA, G,C or A,U-$^{13}$C, $^{15}$N-labeled RNA or uniformly $^{15}$N-labeled RNA. Nonexchangeable proton resonances were assigned from [$^1$H,$^1$H]-NOESY spectra, typically recorded with a mixing time of 250 ms at 298 K, in 100% $D_2O$. Suppression of the residual water signal was achieved by presaturation pulses. Exchangeable proton resonances were assigned using [$^1$H,$^1$H]-NOESY spectra with a WATERGATE pulse sequence for water suppression recorded in 90% $H_2O$/10% $D_2O$ at 278 K. To aid assignment, F1,F2-filtered [$^1$H,$^1$H]-NOESY spectra of G,C $^{13}$C, $^{15}$N-labeled CPEB3 samples were recorded. $^{15}$N resonances of CPEB3 were assigned from [$^1$H,$^{15}$N]-TROSY spectra recorded at 278 K in 90% $H_2O$/10% $D_2O$. Base pair formation was verified by recording $J_{NN}$ HNN-COSY spectra at 278 K in 90% $H_2O$/10% $D_2O$ (Dingley and Grzesiek 1998), which also helped to assign hydrogen bonded $^{15}$N resonances in nucleobases. 4,4-dimethyl-4-silapentane-1-sulfonic acid (DSS) was used as an external, direct reference for $^1$H resonances and as an external, indirect reference for $^{13}$C and $^{15}$N resonances (Markley et al. 1998). Spectra were processed with TopSpin 3.0 (Bruker BioSpin), and assignments were carried out in Sparky (http://www.cgl.ucsf.edu/home/sparky/).

## $Mg^{2+}$ and $[Co(NH_3)_6]^{3+}$ titrations

For metal-ion titrations, a 0.4–0.9 mM of partially deuterated CPEB3 and four samples with only one natural abundance nucleotide (with the remaining three being fully deuterated) were titrated at 298 K with $MgCl_2$ in steps of 0, 0.5, 1, 1.5, 2, 2.5, 3.5, 5, 9, and 18 mM and a [$^1$H,$^1$H]-NOESY spectrum of the exchangeable (recorded at 278 K, sample in 90% $H_2O$ and 10% $D_2O$) and of nonexchangeable (recorded at 298 K, sample in 100% $D_2O$) proton regions were recorded at each step. In addition, a [$^1$H,$^1$H]-NOESY spectrum with an excitation sculpting pulse sequence for water suppression was recorded in the presence of 1.5 mM and 2.5 mM $[Co(NH_3)_6]Cl_3$ at 298 K. Cross peaks between RNA protons and $[Co(NH_3)_6]^{3+}$ protons were assigned in each spectrum. $Mg^{2+}$-induced chemical shift perturbations of the nonexchangeable protons of the P1 and P2 model constructs were determined as described for the full-length CPEB3, titrating samples with increasing amounts of $MgCl^2$ (0, 0.5, 1.5, 3, and 5 mM for P1 and 0, 1, 2, 3, 5, and 7 mM for P2). $Mg^{2+}$-induced chemical shift perturbations of the exchangeable protons of the P2 model construct were obtained by titrating a sample with increasing amounts of $MgCl_2$ (0, 1, 2, 3, 4, 5, 6.5, 8, 9 mM), recording a 1D-$^1$H spectrum in each step.

$K^+$- and $Mg^{2+}$-induced changes of the hydrodynamic radius of CPEB3 were determined by titrating a sample with increasing amount of KCl and $MgCl_2$ (0, 10, 100 mM of KCl plus 2, 5, 10, 20 mM of $MgCl_2$) recording a DOSY experiment at each step and calculating $D$ and $r_H$ for each concentration. Prior to data acquisition, the pD was readjusted after having reached 100 mM KCl, and 10 and 20 mM $MgCl_2$, respectively. In addition, the RNA was reannealed after both additions of KCl. DOSY experiments with excitation sculpting water suppression were recorded with a diffusion delay Δ of 400 msec and a gradient duration $d$ of 2 msec at 298 K in $D_2O$. The gradient strength was raised incrementally from 1.7 to 32.4 G/cm in 56 steps. The peak areas at each gradient strength were determined in TopSpin (Bruker Biospin AG). By plotting $A_0$ against the square of the gradient strength ($G_z$) and fitting to a straight line, the diffusion coefficient can be obtained from

$$\ln\frac{A}{A_{0^-}} = -D\gamma^2 G_z^2 d^2\left(\Delta - \frac{d}{3}\right),$$

where $\gamma = 2.675222005 \times 10^{-8}$ $rad^{-1}$ $T^{-1}$ is the proton gyromagnetic ratio. The hydrodynamic radius is then calculated according to the Stokes-Einstein equation

$$r_H = \frac{k_B T}{6\pi\eta D},$$

where $k_B = 1.3806488 \times 10^{-23}$ J/K is the Boltzmann constant and $\eta_{D2O} = 1.0998$ mPa is the viscosity of $D_2O$.

## $Tb^{3+}$-induced cleavage reactions

The 5′-triphosphates resulting from in vitro transcription of CPEB3 RNA had to be removed prior to 5′-end labeling with $^{32}$P. CPEB3 RNA was dephosphorylated using thermosensitive shrimp alkaline phosphatase (TSAP) in aliquots of 60 pmol/50 µL by adding 5 µL TSAP (1U/µL) and incubating at 37°C for 30 min at 300 rpm. Additional 3 µL of TSAP was added after 15 min. Two rounds of standard phenol–chloroform extraction and subsequent ethanol precipitation were performed to remove the TSAP. The RNA pellet was dissolved in a buffer of 10 mM MOPS, 1 µM EDTA, pH 6.5.

For $^{32}$P radiolabeling, 480 pmol of dephosphorylated CPEB3 in 31 µL ME-buffer was mixed with 4.5 µL T4 polynucleotide kinase and 4.5 µL of the commercial kinase buffer (5×), and 5 µL of $^{32}$P-γ-ATP (6000 Ci/mmol, 150 mCi/mL) to a total volume of 45 µL. Phosphorylation was left to proceed for 30 min at 37°C and 300 rpm and then quenched by adding 45 µL of formamide loading buffer (82% formamide, 10 mM EDTA, pH 8, 0.16% xylene cyanol, 0.16% bromophenol blue). $^{32}$P-labeled CPEB3 was purified by 8% PAGE. The CPEB3 RNA band was visualized by phosphorimaging, excised, crushed, and mixed with crush and soak buffer (10 mM

MOPS, 1 mM EDTA, 250 mM NaCl, pH 6.5). The RNA was eluted into the buffer by shaking for 90 min at 4°C. The supernatant was precipitated with ethanol to recover the RNA. The amount of radiolabeled CPEB was determined by scintillation counting.

For $Tb^{3+}$-induced cleavage reactions, 2.4–2.5 nM of the $^{32}$P-labeled CPEB3 RNA were refolded in 25 mM MOPS (pH 7), 100 mM KCl. One micromole of cold CPEB3 RNA was added to reduce the extent of nonspecific RNA degradation by $Tb^{3+}$ and to facilitate RNA precipitation (Harris and Walter 2003). For annealing, the RNA was heated to 90°C for 90 s, then transferred to ice and 5 or 20 mM $MgCl_2$ was added immediately. Refolding was left to proceed for at least 15 min on ice. $Tb^{3+}$-induced cleavage was carried out in aliquots containing typically 22.5 fmol of refolded $^{32}$P-labeled CPEB3 RNA. An increasing amount of $TbCl_3$ [0–100 µM, in 5 mM sodium(I) cacodylate, pH 5.5], was added to each aliquot and the mixtures were incubated for 30 min at RT. Cleavage reactions were quenched by adding a mixture of 82% formamide and 10 mM EDTA at a 1:1 ratio to each aliquot and by subsequent ethanol precipitation of the cleaved CPEB3 RNA. The RNA fragments were separated by 16% denaturing PAGE and visualized on a phosphorimager. On each gel, an alkaline hydrolysis ladder ($OH^-$) and a T1-ribonuclease cleavage ladder of CPEB3 were loaded (Harris and Walter 2003). The $OH^-$ ladder was prepared by incubating the same amount of radiolabeled CPEB3 as used in the $Tb^{3+}$-induced cleavage reactions in 50 mM sodium carbonate buffer (pH 9) and 1 mM EDTA for 4–5 min at 90°C and by quenching with formamide loading buffer (1:1). The T1 ladder was generated by incubation of the same amount of CPEB3 with 0.1 U/µL T1 in 25 mM sodium citrate buffer (pH 5), 55%–60% formamide, ~7 mM EDTA at 55°C for 4–5 min. T1 digestion was quenched by adding a 7:3 mixture of water/formamide loading buffer (1:1).

## $Mg^{2+}$ counting with 8-hydroxyquinoline-5-sulfonic acid (HQS)

The $Mg^{2+}$-dependent indicator dye 8-hydroxyquinoline-5-sulfonic acid (HQS) served as a $Mg^{2+}$ chelator and a fluorescent reporter at the same time ($Mg^{2+}$ binds to HQS at a 1:1 ratio, strongly enhancing emission at 550 nm). Measurements with HQS were carried out at 298 K on a Varian Carry Eclipse Fluorescence Spectrometer at pH 7, with excitation wavelength 400 nm and with emission wavelength 550 nm (as previously described by Romer and Hach 1975; Grilley et al. 2009). Two samples (0.1 mM HQS, 20 mM MOPS buffer, 50 mM, 100 mM, or 2 M KCl), one of which contained 24 µM of CPEB3 RNA, were titrated with $Mg^{2+}$ in exactly the same way (2–260 µM $Mg^{2+}$) in 29–42 steps. In the second sample, CPEB3 ribozyme (annealed by a 2-min heating at 90°C and rapidly cooled on ice to ensure the proper folding) was present. After each $MgCl_2$ addition, the sample was mixed thoroughly and the fluorescence intensity at 550 nm was recorded.

The effect of the concentration of $K^+$ ions on $Mg^{2+}$ association to the RNA was found to be negligible in the measured range of ionic strength; experiments carried out at monovalent ion concentration similar to physiological (50 and 100 mM KCl) were repeated three times and the control experiment at 2 M KCl was performed twice. By plotting the difference in fluorescence intensities between the blank and CPEB3/containing samples against the ratio between [$Mg^{2+}$] and [CPEB3], a plateau is reached when the equivalent of $Mg^{2+}$ binding to the RNA has been added. Fluorescence spectra did not change with increased exposure to photoexcitation or longer sample mixing, indicating that photobleaching of HQS can be neglected. The equilibration of the sample was fast and longer waiting times between $Mg^{2+}$ additions did not result in a change of fluorescence.

## $Mg^{2+}$ counting with atomic emission spectroscopy

Measurements were performed as previously described in the literature (Bina-Stein and Stein 1976; Leipply et al. 2009). Tube-O-DIALYZER Micro filters with a 1-kDa molecular weight cut-off were used to dialyze the ribozyme samples overloaded with $Mg^{2+}$-containing buffer (20 mM MOPS buffer, pH 7, 50 mM, 100 mM, or 2 M KCl and 0.5–100 mM $Mg^{2+}$, 24 µM CPEB3 ribozyme, annealed by a 2-min heating at 90°C and rapid cooling on ice; the total volume of the dialyzed sample was 100 µL) against 5 mL of the same buffer without $Mg^{2+}$ ions for 4–10 h at 298 K. The concentration of $Mg^{2+}$ in the dialysate was measured with AAS on a Varian SpectraAA 110 spectrometer, and the amount of $Mg^{2+}$ ions bound to the ribozyme was calculated as the ratio between the difference of the amount of $Mg^{2+}$ added and present in the dialysate and the amount of CPEB3.

## SUPPLEMENTAL MATERIAL

Supplemental material is available for this article.

## ACKNOWLEDGMENTS

Financial support from a Marie Curie fellowship (PIEFGA-2012–329700 to M.R.-Z.), the Swiss National Science Foundation (to R.K.O.S.), and the University of Zurich is gratefully acknowledged. R.K.O.S. is a recipient of an ERC Starting Grant (MIRNA). We wish to thank Susann Paulus for quantification of the Tb(III) cleavage data, as well as Daniela Donghi and Silke Johannsen for critical remarks and helpful suggestions on this manuscript.

*Received August 8, 2015; accepted January 4, 2016.*

## REFERENCES

Bina-Stein M, Stein A. 1976. Allosteric interpretation of $Mg^{2+}$ ion binding to the denaturable *Escherichia coli* tRNAGlu2. *Biochemistry* **15:** 3912–3917.

Chadalavada DM, Gratton EA, Bevilacqua PC. 2010. The human HDV-like CPEB3 ribozyme is intrinsically fast-reacting. *Biochemistry* **49:** 5321–5330.

Chen JH, Yajima R, Chadalavada DM, Chase E, Bevilacqua PC, Golden BL. 2010. A 1.9 Å crystal structure of the HDV ribozyme precleavage suggests both Lewis acid and general acid mechanisms contribute to phosphodiester cleavage. *Biochemistry* **49:** 6508–6518.

Chen J, Ganguly A, Miswan Z, Hammes-Shiffer S, Bevilacqua PC. 2013. Identification of the catalytic $Mg^{2+}$ ion in the hepatitis delta virus ribozyme. *Biochemistry* **52:** 557–567.

Choudhary PK, Gallo S, Sigel RKO. 2014. Monitoring global structural changes and specific metal binding sites in RNA by in-line probing and Tb(III) cleavage. *Methods Mol Biol* **1086:** 143–158.

Christerson LB, McKearin DM. 1994. *orb* is required for anteroposterior and dorsoventral patterning during *Drosophila* oogenesis. *Gene Dev* **8:** 614–628.

Ciesiolka J, Wrzesinski J, Gornicki P, Podkowinski J, Krzyzosiak W. 1989. Analysis of magnesium, europium and lead binding-sites in methionine initiator and elongator transfer-RNAs by specific metal-ion-induced cleavages. *Eur J Biochem* **186:** 71–77.

Darnell JC, Richter JD. 2012. Cytoplasmic RNA-binding proteins and the control of complex brain function. *Perspect Biol* **4:** a012344.

Das R, Travers KJ, Bai Y, Herschlag D. 2005. Determining the $Mg^{2+}$ stoichiometry for folding an RNA metal ion core. *J Am Chem Soc* **127:** 8272–8273.

de la Pena M, Garcia-Robles I. 2010. Intronic hammerhead ribozymes are ultraconserved in the human genome. *EMBO Rep* **11:** 711–716.

Dingley AJ, Grzesiek S. 1998. Direct observation of hydrogen bonds in nucleic acid base pairs by internucleotide $2J_{NN}$ couplings. *J Am Chem Soc* **120:** 8293–8297.

Dye MJ, Gromak N, Proudfoot NJ. 2006. Exon tethering in transcription by RNA polymerase II *Mol. Cell* **21:** 849–859.

Eimer W, Williamson JR, Boxer SG, Pecora R. 1990. Characterization of the overall and internal dynamics of short oligonucleotides by depolarized dynamic light scattering and NMR relaxation measurements. *Biochemistry* **29:** 799–811.

Erat MC, Sigel RKO. 2011. Methods to detect and characterize metal ion binding sites in RNA. *Met Ions Life Sci* **9:** 37–100.

Ferre-D'Amare AR, Zhou K, Doudna JA. 1998. Crystal structure of a hepatitis delta virus ribozyme. *Nature* **395:** 567–574.

Freisinger E, Sigel RKO. 2007. From nucleotides to ribozymes—a comparison of their metal ion binding properties. *Coord Chem Rev* **251:** 1834–1851.

Gallo S, Furler M, Sigel RKO. 2005. In vitro transcription and purification of RNAs of different size. *Chimia* **59:** 812–816.

Glasoe PK, Long FA. 1960. Use of glass electrodes to measure acidities in deuterium oxide. *J Phys Chem* **64:** 188–190.

Gong B, Chen JH, Chase E, Chadalavada DM, Yajima R, Golden BL, Bevilacqua PC, Carey PR. 2007. Direct measurement of a pK(a) near neutrality for the catalytic cytosine in the genomic HDV ribozyme using Raman crystallography. *J Am Chem Soc* **129:** 13335–13342.

Gong B, Chen JH, Bevilacqua PC, Golden BL, Carey PR. 2009. Competition between $Co(NH_3)_6^{3+}$ and inner sphere $Mg^{2+}$ ions in the HDV ribozyme. *Biochemistry* **48:** 11961–11970.

Grilley D, Soto AM, Draper DE. 2009. Direct quantitation of $Mg^{2+}$-RNA interactions by use of a fluorescent dye. *Methods Enzymol* **455:** 71–94.

Harris DA, Walter NG. 2003. Probing RNA structure and metal-binding sites using terbium(III) footprinting. *Curr Protoc Nucleic Acid Chem* **6.8:** 6.8.1–6.8.8.

Jeng KS, Daniel A, Lai MM. 1996. A pseudoknot ribozyme structure is active in vivo and required for hepatitis delta virus RNA replication. *J Virol* **70:** 2403–2410.

Kapral G, Jain S, Noeske J, Doudna JA, Richardson DC, Richardson JS. 2014. New tools provide a second look at HDV ribozyme structure, dynamics and cleavage. *Nucl Acids Res* **42:** 12833–12846.

Kayne MS, Cohn M. 1974. Enhancement of terbium(III) and europium(III) fluorescence in complexes with *Escherichia coli* tRNA. *Biochemistry* **13:** 4159–4165.

Ke A, Zhou K, Ding F, Cate JHD, Doudna JA. 2004. A conformational switch controls hepatitis delta virus ribozyme catalysis. *Nature* **429:** 201–205.

Krasovska MV, Sefcikova J, Reblova K, Schneider B, Walter NG, Sponer J. 2006. Cations and hydration in catalytic RNA: molecular dynamics of the Hepatitis Delta Virus ribozyme. *Biophys J* **91:** 626–638.

Lantz V, Chang JS, Horabin JI, Bopp D, Schedl P. 1994. The *Drosophila* orb RNA-binding protein is required for the formation of the egg chamber and establishment of polarity. *Gene Dev* **8:** 598–613.

Lapham J, Rife JP, Moore PB, Crothers DM. 1997. Measurement of diffusion constants for nucleic acids by NMR. *J Biomol NMR* **10:** 255–262.

Leipply D, Lambert D, Draper DE. 2009. Ion-RNA interactions: thermodynamic analysis of the effects of mono- and divalent ions on RNA conformational equilibria. *Methods Enzymol* **469:** 433–463.

Luitjens C, Gallegos M, Kraemer B, Kimble J, Wickens M. 2000. CPEB proteins control two key steps in spermatogenesis in *C. elegans*. *Gene Dev* **14:** 2596–2609.

Macnaughton TB, Wang YJ, Lai MM. 1993. Replication of hepatitis delta virus RNA: effect of mutations of the autocatalytic cleavage sites. *J Virol* **67:** 2228–2234.

Markley JL, Bax A, Arata Y, Hilbers CW, Kaptein R, Sykes BD, Wright PE, Wurthrich K. 1998. Recommendations for the presentation of NMR structures of proteins and nucleic acids. IUPAC-IUBMB-IUPAB Inter-Union Task Group on the Standardization of Data Bases of Protein and Nucleic Acid Structures Determined by NMR Spectroscopy. *J Biomol NMR* **12:** 1–23.

Martick M, Horan LH, Noller HF, Scott WG. 2008. A discontinuous hammerhead ribozyme embedded in a mammalian messenger RNA. *Nature* **454:** 899–902.

Murray JB, Seyhan AA, Walter NG, Burke JM, Scott WG. 1998. The hammerhead, hairpin and VS ribozymes are catalytically proficient in monovalent cations alone. *Chem Biol* **5:** 587–595.

Nakano SI, Proctor DJ, Bevilacqua PC. 2001. Mechanistic characterization of the HDV genomic ribozyme: assessing the catalytic and structural contributions of divalent metal ions within a multichannel reaction mechanism. *Biochemistry* **40:** 12022–12038.

Nehdi A, Perreault JP. 2006. Unbiased in vitro selection reveals the unique character of the self-cleaving antigenomic HDV RNA sequence. *Nucleic Acids Res* **34:** 584–592.

Nix JC, Newhoff AR, Wilson C. 1999. Preliminary crystallographic characterization of an in vitro evolved biotin-binding RNA pseudoknot. *Acta Crystallogr D Biol Crystallogr* **55:** 323–325.

Perrotta AT, Been MD. 1991. A pseudoknot-like structure required for efficient self-cleavage of hepatitis delta virus RNA. *Nature* **350:** 434–436.

Riccitelli NJ, Delwart E, Luptak A. 2014. Identification of minimal HDV-like ribozymes with unique divalent metal ion dependence in the human microbiome. *Biochemistry* **53:** 1616–1626.

Richter JD. 2007. CPEB: a life in translation. *Trends Biochem Sci* **32:** 279–285.

Robinson H, Wang AHJ. 1996. Neomycin, spermine and hexaamminecobalt(III) share common structural motifs in converting B- to A-DNA. *Nucleic Acids Res* **24:** 676–682.

Romer R, Hach R. 1975. tRNA conformation and magnesium binding. A study of a yeast phenylalanine-specific tRNA by a fluorescent indicator and differential melting curves. *Eur J Biochem* **55:** 271–284.

Rowinska-Zyrek M, Skilandat M, Sigel RKO. 2013. Hexaamminecobalt (III)—probing metal ion binding sites in nucleic acids by NMR spectroscopy. *Z Anorg Allg Chem* **639:** 1313–1320.

Salehi-Ashtiani K, Luptak A, Litovchick A, Szostak JW. 2006. A genome-wide search for ribozymes reveals an HDV-like sequence in the human CPEB3 gene. *Science* **313:** 1788–1792.

Sigel RKO, Pyle AM. 2003. Lanthanide ions as probes for metal ions in the structure and catalytic mechanism of ribozymes. *Met Ions Biol Syst* **40:** 477–512.

Sigel RKO, Pyle AM. 2007. Alternative roles for metal ions in enzyme catalysis and the implications for ribozyme chemistry. *Chem Rev* **107:** 97–113.

Skilandat M, Rowinska-Zyrek M, Sigel RKO. 2014. Solution structure and metal ion binding sites of the human CPEB3 ribozyme's P4 domain. *J Biol Inorg Chem* **6:** 903–912.

Soukup GA, Breaker RR. 1999. Relationship between internucleotide linkage geometry and the stability of RNA. *RNA* **5:** 1308–1325.

Strulson CA, Yennawar NH, Rambo RP, Bevilacqua PC. 2013. Molecular crowding favors reactivity of a human ribozyme under physiological ionic conditions. *Biochemistry* **52:** 8187–8197.

Tanaka Y, Hori T, Tagaya M, Sakamoto T, Kurihara Y, Katahira M, Uesugi S. 2002. Imino proton NMR analysis of HDV ribozymes: nested double pseudoknot structure and $Mg^{2+}$ ion-binding site close to the catalytic core in solution. *Nucleic Acids Res* **30:** 766–774.

Teixeira A, Tahiri-Alaoui A, West S, Thomas B, Ramadass A, Martianov I, Dye M, James W, Proudfoot NJ, Akoulitchev A. 2004. Autocatalytic RNA cleavage in the human ß-globin pre-mRNA promotes transcription termination. *Nature* **432:** 526–530.

Thaplyal P, Ganguly A, Golden BL, Hammes-Shiffer S, Bevilacqua PC. 2013. Thio effects and an unconventional metal ion rescue in the genomic hepatitis delta virus ribozyme. *Biochemistry* **52:** 6499–6514.

Veeraraghavan N, Ganguly A, Golden BL, Bevilacqua PC, Hammes-Schiffer S. 2011. Mechanistic strategies in the HDV ribozyme: chelated and diffuse metal ion interactions and active site protonation. *J Phys Chem B* **115:** 8346–8357.

Vogler C, Spalek K, Aerni A, Demougin P, Muller A, Huynh KD, Papassotiropoulos A, de Quervain DJ. 2009. CPEB3 is associated with human episodic memory. *Front Behav Neurosci* **3:** 4.

Wadkins TS, Perrotta AT, Ferré-D'Amaré AR, Doudna JA, Been MD. 1999. A nested double pseudoknot is required for self-cleavage activity of both the genomic and antigenomic hepatitis delta virus ribozymes. *RNA* **5:** 720–727.

Webb CHT, Luptak A. 2011. HDV-like self-cleaving ribozymes. *RNA Biol* **8:** 719–727.

Webb CHT, Riccitelli NJ, Ruminski DJ, Luptak A. 2009. Widespread occurrence of self-cleaving ribozymes. *Science* **326:** 953.